Three-dimensional femtosecond laser nanolithography of crystals

Airán Ródenas [1]*, Min Gu[2], Giacomo Corrielli[1], Petra Paiè[1], Sajeev John[3], Ajoy K. Kar[4] and Roberto Osellame [1]

So far, nanostructuring of hard optical crystals has been exclusively limited to their surface, as stress-induced crack formation and propagation render high-precision volume processes ineffective[1,2]. Here, we show that the rate of nanopore chemical etching in the popular laser crystals yttrium aluminium garnet and sapphire can be enhanced by more than five orders of magnitude (from <0.6 nm h^{-1} to ~100 µm h^{-1}) by the use of direct laser writing, before etching. The process makes it possible to produce arbitrary three-dimensional nanostructures with 100 nm feature sizes inside centimetre-scale laser crystals without brittle fracture. To showcase the potential of the technique we fabricate subwavelength diffraction gratings and nanostructured optical waveguides in yttrium aluminium garnet and millimetre-long nanopores in sapphire. The approach offers a pathway for transferring concepts from nanophotonics to the fields of solid-state lasers and crystal optics.

The optical properties of a material are known to depend not only on its chemistry but also on its subwavelength structure. With the inception of the photonic crystal[3,4] and metamaterial[5,6] concepts this idea proved to be key to access a new level of light manipulation beyond what is allowed by the natural optical properties of materials. However, in over three decades of research, no technique has been able to reliably nanostructure optical crystals beyond their surface.

Laser lithography, as developed by the semiconductor industry, is a surface processing technique that exploits the efficient etching of a range materials (such as silicon, silica glass or polymers) to produce high-quality two-dimensional (2D) nanophotonic devices[7,8]. Its extension from 2D to 3D was demonstrated two decades ago with infrared femtosecond laser direct writing to introduce multiphoton absorption in a resin photo-polymerization process[9]. This approach prompted seminal demonstrations of lithographically produced 3D photonic crystals for the optical range, first made of pure polymerized material[10–12], and later silicon and other optical materials by means of further processing steps[13,14]. The technological exploitation of photo-polymerized structures has, however, proven to be impractical because they cannot be efficiently interfaced with other photonic elements. A remarkable example of the potential of 3D nanostructuring of macroscopic optical materials comes from the field of optical fibres, where photonic crystal fibres have delivered functionalities that go far beyond what is feasible with ordinary unstructured glass[15,16] and have revolutionized the areas of nonlinear optics and optical communications[17–19]. Yet, their manufacturing in crystalline media has remained elusive due to the difficulty of applying stack and drawing techniques with crystals. The prospects of directly machining 3D nanostructures by laser-induced dielectric breakdown also

led to reports that amorphous and void submicrometre structures can be induced in crystals, although at the cost of imparting high-pressure waves, which lead to extended lattice damage and crack propagation[20,21]. Despite efforts, no method has been reported for the large-scale 3D volume nanostructuring of a crystal.

Departing from prevailing approaches, we propose that the inner chemical reactivity of a crystal, given by its wet etch rate, can be locally modified at the nanometre scale, and dense nanopore lattices can be formed by means of multiphoton 3D laser writing (3DLW). We show that centimetre-long empty pore lattices with arbitrary feature sizes at the 100 nm level can be created inside the key crystals used in many applications (such as yttrium aluminium garnet (YAG) and sapphire). Processing is performed by direct laser writing of the desired pore architecture inside the crystal, polishing the sample to expose the terminations of the written tracks, and chemically etching the irradiated material. An etching selectivity larger than 1×10^5, never observed before in a photo-irradiated material, is achieved between the modified and pristine crystalline states. This allows the design and fabrication of nanophotonic elements inside a crystal that provide optical responses determined by their subwavelength structure.

To achieve volume nanostructuring of crystals at a large scale it is necessary to arrange nanopores in arbitrary close-packed structures at macroscopic lengths (millimetre to centimetre scale) without causing brittle fracture of the crystal due to excessive stress accumulation. In addition, pores have to be written in arbitrary directions, their size must be controlled with at least ~10 nm reproducibility to achieve functional nanophotonic devices, and the pore cross-sectional shape must be tailorable.

We show that all these features (pore direction, size, shape, filling fraction and length) can be controlled by combining 3DLW and wet etching. Figure 1 summarizes the controlled creation of nanopore lattices in YAG crystals. No dependence on the crystalline axis was found for the pore size and wet etching rate within our experimental resolution, so an arbitrary reference frame was set where the x and y axes define the pore's cross-sectional plane, and z is defined along the pore length axis. Figure 1a shows a 1-mm-long lattice of nanopores arranged in a centred orthogonal symmetry with 1 µm in-plane spacing. The lattice was etched for 120 h (see Methods) and the average pore dimensions were 257 ± 7 nm and 454 ± 13 nm in the x and y directions, respectively. Control over the pore shape and size can be performed by tailoring the laser power and polarization (Supplementary Fig. 1), but to achieve bespoke pore shapes for constant laser power the overlapping of pores was also tested. Figure 1b presents an array of parallel pores that were

[1]Istituto di Fotonica e Nanotecnologie, Consiglio Nazionale delle Ricerche, Milan, Italy. [2]Laboratory of Artificial-Intelligence Nanophotonics, School of Science, Royal Melbourne Institute of Technology, Melbourne, Victoria, Australia. [3]Department of Physics, University of Toronto, Toronto, Ontario, Canada. [4]Institute of Photonics and Quantum Sciences, David Brewster Building, Heriot-Watt University, Edinburgh, UK. *e-mail: arodenas@gmail.com
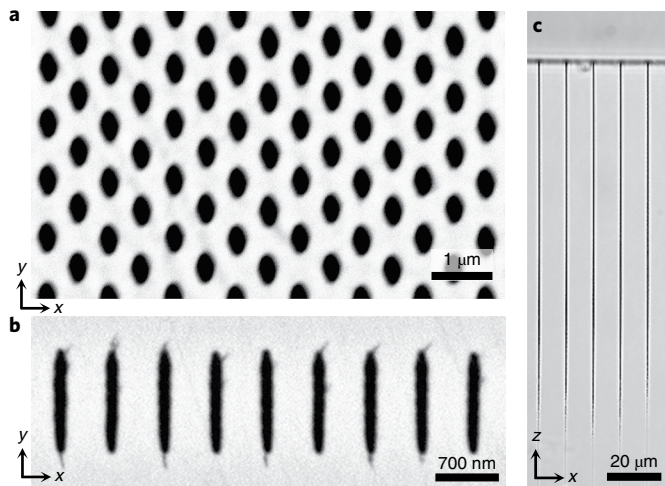
Fig. 1 | Wet etching of nanopore lattices fabricated by 3DLW in YAG.
a, Nanopore lattice etched for 120 h with average pore dimensions of 257 ± 7 nm and 454 ± 13 nm along the x and y reference axes, and 1 mm lengths along z. **b**, Vertically overlapping nanopores after 2 h wet etching (average dimensions of 131 ± 5 nm and $1,300 \pm 35$ nm along x and y, and 1 mm lengths). **c**, Top optical microscope view of nanopores (129 ± 6.8 μm length) along the z direction, etched for 1 h.

vertically stacked to achieve arbitrarily elongated cross-sections. Pores in this experiment were etched for 2 h and had an average size of 131 ± 5 nm and $1,300 \pm 35$ nm along the x and y axes, respectively. The etching of crossing pores along different directions was also studied to prove the 3D nature of the lithographic process. Supplementary Fig. 2 shows pores that crisscross at 90° angles and at different relative depths within the crystal.

The creation of air-pore photonic lattices makes it possible to achieve nanophotonic structures inside a crystal, with a spatial resolution equivalent to state-of-the-art multiphoton polymerization lithography[22]. However, the use of nanophotonic devices in practical scenarios requires robust and efficient optical interconnections and capability for the design of large and complex circuits. To achieve this, it is essential to maintain the spatial resolution and lattice fidelity across large footprints on a mm² scale or beyond. The critical parameter that enables such control over large pore lengths is the differential etching rate between the photo-modified volumes and the surrounding crystal. Figure 1c presents a top-view optical microscope image of an array of 200 nm nanopores etched for 1 h. The large refractive index contrast between the air and crystal allows us to determine a pore length of ~129 μm and thus an averaged nanopore etch rate of 129 ± 6.8 μm h⁻¹ for the first hour of etching. The slow etching rate of unmodified YAG was determined to be <1 nm h⁻¹ (0.36 ± 0.23 nm h⁻¹) from the average of all experiments performed in our wet etching conditions (see Methods). The 1 h average etching selectivity of 3DLW YAG nanopores is thus determined to be greater than 1×10^5 ($3.6 \pm 2.5 \times 10^5$), the highest value ever observed for any lithographic process so far, and approximately two orders of magnitude higher than that of alumina over silicon[23]. Due to this high selectivity, nanopores with cross-sections of 368×726 nm² and lengths of 3.1 mm were achieved by etching for 170 h from both end sides of the pores (Supplementary Fig. 3), showing that nanopores with millimetre-scale lengths are feasible with one single etching step. Furthermore, to homogeneously etch longer nanostructures on the centimetre scale (or potentially beyond), as well as to keep the etching times as short as a few hours, a scheme for vertical-access etching of pores was implemented, thus allowing the achievement of structures with arbitrary length across the whole sample (Supplementary Fig. 4).
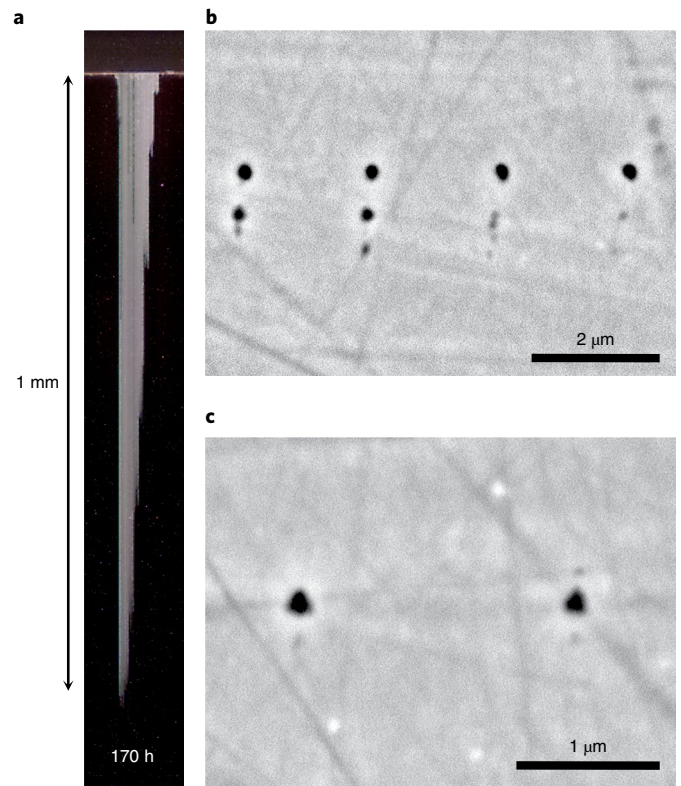
Fig. 2 | Etching of mm-long nanopores in sapphire. a, Dark-field image of three arrays of 1-mm-long pores after 170 h of total etching time. Pores on each array were written at ~10 mW and at depths ranging from 4 to 30 μm. **b**, Example of pores written at medium power (9.4 mW) and 29 μm depth, after 30 min etching. Birefringence-induced focal splitting results in multiple pores along the (top to bottom) in-depth focusing direction. The four main (top) pores have an average width of 197 ± 12 nm and height of 227 ± 9 nm. The two observed second pores have an average width of 154 ± 5 nm and a height of 164 ± 7 nm. **c**, Example of two pores written at 24 μm depth and at the photo-modification power threshold (~4 mW) for which no secondary pores are observed. The pores have an average width of 121 ± 12 nm and height of 135 ± 21 nm.

To evaluate if the observed giant nanopore etching selectivity is restricted to the case of YAG or if it is a phenomenon that can manifest also in other types of crystal, we performed further nanostructuring experiments in sapphire (see Methods). A nanopore etch rate of $\sim 1 \times 10^5$ ($2.3 \pm 1.7 \times 10^5$) was found, similar to that in YAG and more than one order of magnitude larger than previously observed when etching amorphous microchannels in sapphire[21]. Figure 2a shows an image of millimetre-long nanopores formed in sapphire. Cross-sections as small as ~120 nm could be obtained (Fig. 2b,c).

As shown in Fig. 1, the cross-sectional aspect ratio of the pores can be engineered by means of pore overlapping; however, this process inevitably leads to larger pore cross-sections and for some nanophotonic applications symmetric pores at the 100 nm level are required. We show that a route to achieve this is to perform 3DLW at powers close to the threshold for laser photo-modification. Under our 3DLW experimental conditions, ~110 nm nanopores were obtained in YAG with almost circular shapes for circularly polarized laser irradiation (see Supplementary Information). Figure 3a shows a lattice of 1-mm-long nanopores fabricated in YAG with decreasing powers towards deeper layers. The obtained lattice has a slowly varying pore cross-section with widths ranging from ~139 nm to ~109 nm, heights from ~204 nm down to ~132 nm, and aspect ratios ranging from ~1.45 to ~1.20 at different depths. To test the feasibility
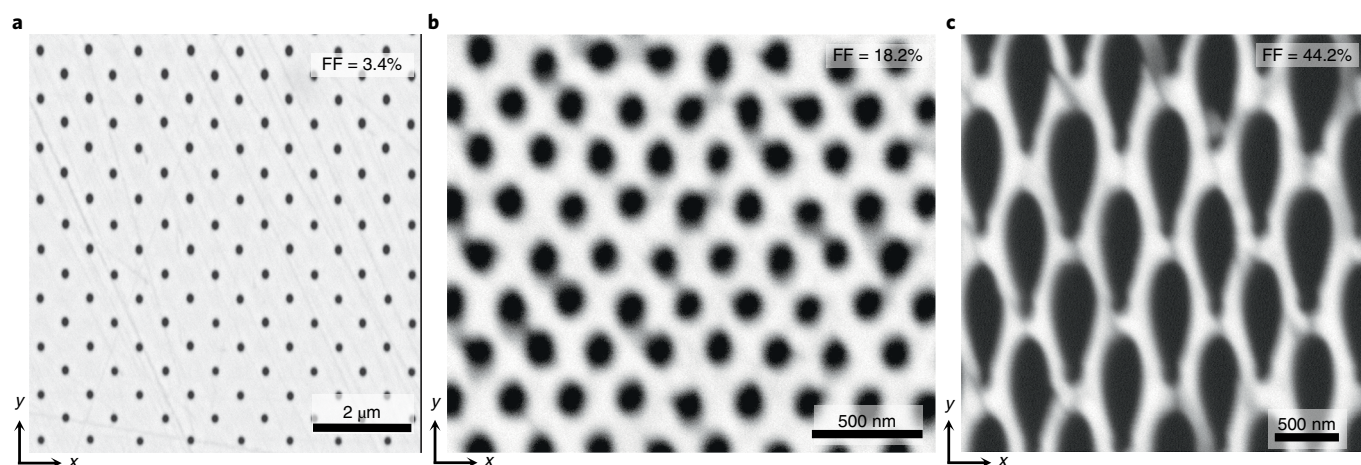
Fig. 3 | 3DLW nanostructures in YAG with 100 nm feature sizes and filling fraction control. a, Low pore filling fraction (FF) lattice (3.4%) written with linearly varying pore size along the depth (top to bottom x widths ranging from 139 ± 4 nm to 109 ± 6 nm, y heights from 204 ± 6 nm to 132 ± 8 nm, and aspect ratio from ~1.45 to ~1.20). **b,** Hexagonal pore lattice with 250 nm spacing and 18.2% pore filling fraction (average x width of 109 ± 8 nm, y height of 125 ± 10 nm and aspect ratio of ~1.15). **c,** High filling fraction (44.2%) pore lattice with ~150 nm crystal walls separating elliptical pores with average cross-sections of 276×972 nm². All pores have ~1 mm lengths.
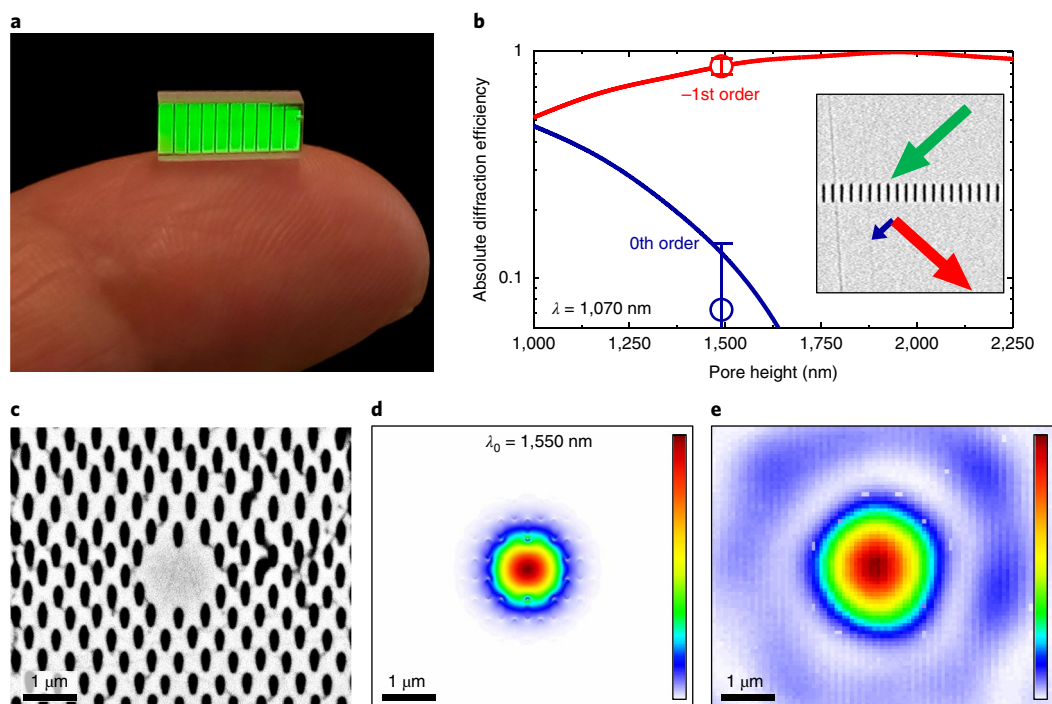
Fig. 4 | Subwavelength diffraction gratings and MOW in YAG crystals. a, Image of a centimetre-long 700 nm pitch grating under visible light illumination. **b,** Experimental and calculated absolute diffraction efficiencies of a subwavelength grating (700 nm pitch) with 1,070 nm wavelength. Efficiency is calculated as the diffracted power divided by the power incident to the embedded grating. Error bars correspond to the experimental s.d. of ~0.07%. Inset, scanning electron microscopy (SEM) close-up image of the fabricated grating. **c,** Optical waveguide with hexagonal structure, 500 nm horizontal pore-to-pore spacing, mean pore size of 166×386 nm² and 4 mm length. **d,** Simulated intensity mode profile at 1,550 nm with FWHMs of 862 nm (vertical) and 972 nm (horizontal). **e,** Diffraction-limited near-field image of the waveguide output mode measured at 1,550 nm, with a FWHM of ~1.5 μm.

of fabricating high-filling-fraction nanopore lattices without fracturing the crystal, hexagonal lattices with lattice spacing down to 250 nm were also fabricated. Figure 3b shows a close-up of such a lattice after etching for 15 h, with an air filling fraction of 18%, average pore diameter of ~117 nm, aspect ratio of ~1.15 and a dielectric wall thickness of ~133 nm between pores. This control over the lattice spacing down to 250 nm could prove useful for designing

photonic bandgap lattices with stopbands in the visible to mid-infrared range[24] inside solid-state laser crystals.

A different route to achieve larger air filling fractions is by etching larger pores. Large air filling fraction structures are also essential for tailoring the properties of photonic crystal and microstructured optical waveguides (MOWs), such as the dispersion, mode size and nonlinear coefficient[15–19]. Reaching a high air filling fraction inside a

crystal requires the fabrication of extended thin crystalline nanolayers without crystal fracture. The creation of such lattices was validated by fabricating a centred orthogonal lattice with in-plane pore spacing of 700 nm and pore cross-sections of 276×972 nm^2 (Fig. 3c), with a 44% air pore filling fraction and ~150 nm dielectric walls in the absence of crack formation, even at the surface after mechanical polishing.

Having established the etching rates and achievable features sizes of the crystalline nanostructures inside YAG, we sought to determine (1) whether the crystal nanopores are indeed void, even millimetres away from the entrant wet etching surface and (2) whether the functional subwavelength nanophotonics elements can indeed be successfully realized on a large scale. To answer the first question, a nanograting with subwavelength pitch (700 nm) was fabricated in YAG to be tested at a wavelength of 1,070 nm (Fig. 4a). The subwavelength grating was designed to produce only the −1st diffraction order. It was fabricated with 10 different laser powers to control the pores' cross-sectional shape, and tested in a Littrow configuration for the highest diffraction efficiency[25]. A total efficiency of 86% was experimentally obtained for the −1st order of the grating having the larger pores cross-section of 165 nm width and 1,520 nm height. Calculations (Methods) assuming air filled pores are shown in Fig. 4b, agreeing well with the measured values and demonstrating that the long etched nanopores are void.

To further evaluate the quality and potential of the 3D nanolithography technique, the fabrication of MOWs with different lattice spacings and cavity sizes was studied (Supplementary Fig. 5). Figure 4c presents a nanostructured waveguide in YAG with core size of 1.1×1.3 μm^2, triangular symmetry cladding with an in-plane spacing of 500 nm, average pore size of 166×386 nm^2 and length of 4 mm. Figure 4d shows the calculated mode at 1,550 nm wavelength for a vertically polarized electric field. The mode is effectively subwavelength with a full-width at half-maximum (FWHM) of ~900 nm (~0.6λ). Figure 4e shows the measured diffraction-limited image of the waveguide output mode for vertical polarization at 1,550 nm (see Supplementary Information). From the calculations the MOW is expected to have a modified dispersion function with two zero dispersion wavelengths (ZDWs) at 0.93 μm and 1.51 μm, well below the natural ZDW of YAG at 1.6 μm (Supplementary Fig. 6), which could allow the development of microcombs[26] pumped with Nd^{3+} and Yb^{3+} ions from the same solid-state laser chip.

Besides novel applications in crystalline 3D nanophotonics and nonlinear optics, the 3D nanostructuring of crystals also opens up new routes to design compact monolithic solid-state lasers incorporating traditional cavity elements (such as mirrors, gratings, metalenses, dispersion elements, fibres and microfluidic cooling channels) or novel microresonators inside a crystal[26]. The possibility of fabricating large nanostructured laser crystals also opens up the potential for new applications in ultrastrong deformable laser nanofibres[27–29].

Online content

Any methods, additional references, Nature Research reporting summaries, source data, statements of data availability and associated accession codes are available at https://doi.org/10.1038/s41566-018-0327-9.

References

1. Gamaly, E. G. et al. Laser–matter interaction in the bulk of a transparent solid: confined microexplosion and void formation. *Phys. Rev. B* **73**, 214101 (2006).
2. Juodkazis, S., Mizeikis, V. & Misawa, H. Three-dimensional microfabrication of materials by femtosecond lasers for photonics applications. *J. Appl. Phys.* **106**, 051101 (2009).
3. John, S. Strong localization of photons in certain disordered dielectric superlattices. *Phys. Rev. Lett.* **58**, 2486 (1987).
4. Yablonovitch, E. Inhibited spontaneous emission in solid-state physics and electronics. *Phys. Rev. Lett.* **58**, 2059 (1987).
5. Shelby, R. A., Smith, D. R. & Schultz, S. Experimental verification of a negative index of refraction. *Science* **292**, 77–79 (2001).
6. Smith, D. R., Pendry, J. B. & Wiltshire, M. C. K. Metamaterials and negative refractive index. *Science* **305**, 788–792 (2004).
7. Jain, K., Willson, C. G. & Lin, B. J. Ultrafast deep UV lithography with excimer lasers. *IEEE Electron Device Lett.* **3**, 53–55 (1982).
8. McGarvey-Lechable, K. et al. Slow light in mass-produced dispersion-engineered photonic crystal ring resonators. *Opt. Express* **25**, 3916–3926 (2017).
9. Maruo, S., Nakamura, O. & Kawata, S. Three-dimensional microfabrication with two-photon-absorbed photopolymerization. *Opt. Lett.* **22**, 132–134 (1997).
10. Straub, M. & Gu, M. Near-infrared photonic crystals with higher-order bandgaps generated by two-photon photopolymerization. *Opt. Lett.* **27**, 1824–1826 (2002).
11. Deubel, M. et al. Direct laser writing of three-dimensional photonic-crystal templates for telecommunications. *Nat. Mater.* **3**, 444–447 (2004).
12. Wong, S. et al. Direct laser writing of three-dimensional photonic crystals with a complete photonic bandgap in chalcogenide glasses. *Adv. Mater.* **18**, 265–269 (2006).
13. Hermatschweiler, M., Ledermann, A., Ozin, G. A., Wegener, M. & von Freymann, G. Fabrication of silicon inverse woodpile photonic crystals. *Adv. Funct. Mater.* **17**, 2273–2277 (2007).
14. Gansel, J. K. et al. Gold helix photonic metamaterial as broadband circular polarizer. *Science* **325**, 1513–1515 (2009).
15. Knight, J. C., Birks, T. A., Russell, P., St., J. & Atkin, D. M. All-silica single-mode optical fiber with photonic crystal cladding. *Opt. Lett.* **21**, 1547–1549 (1996).
16. Russell, P. Photonic crystal fibers. *Science* **299**, 358–363 (2003).
17. Dudley, J. M., Genty, G. & Coen, S. Supercontinuum generation in photonic crystal fiber. *Rev. Mod. Phys.* **78**, 1135–1184 (2006).
18. Rarity, J. G. et al. Photonic crystal fiber source of correlated photon pairs. *Opt. Express* **13**, 534–544 (2005).
19. Francis-Jones, R. J. A., Hoggarth, R. A. & Mosley, P. J. All-fiber multiplexed source of high-purity single photons. *Optica* **3**, 1270–1273 (2016).
20. Glezer, E. N. & Mazur, E. Ultrafast-laser driven micro-explosions in transparent materials. *Appl. Phys. Lett.* **71**, 882–884 (1997).
21. Juodkazis, S. et al. Control over the crystalline state of sapphire. *Adv. Mater.* **18**, 1361–1364 (2006).
22. Fischer, J. et al. Three-dimensional multi-photon direct laser writing with variable repetition rate. *Opt. Express* **21**, 26244–26260 (2013).
23. Henry, M. D., Walavalkar, S., Homyk, A. & Scherer, A. Alumina etch masks for fabrication of high-aspect-ratio silicon micropillars and nanopillars. *Nanotechnology* **20**, 255305 (2009).
24. Joannopoulos, J. D., Villeneuve, P. R. & Fan, S. Photonic crystals: putting a new twist on light. *Nature* **386**, 143–149 (1997).
25. Clausnitzer, T. et al. Highly-dispersive dielectric transmission gratings with 100% diffraction efficiency. *Opt. Express* **16**, 5577–5584 (2008).
26. Kippenberg, T. J., Gaeta, A. L., Lipson, M. & Gorodetsky, M. L. Dissipative Kerr solitons in optical microresonators. *Science* **361**, 6402 (2018).
27. Meza, L. R., Das, S. & Greer, J. R. Strong, lightweight, and recoverable three-dimensional ceramic nanolattices. *Science* **345**, 1322–1326 (2014).
28. Bauer, J., Schroer, A., Schwaiger, R. & Kraft, O. Approaching theoretical strength in glassy carbon nanolattices. *Nat. Mater.* **15**, 438–443 (2016).
29. Banerjee, A. et al. Ultralarge elastic deformation of nanoscale diamond. *Science* **360**, 300–302 (2018).

Acknowledgements

Author contributions

The investigation was carried out by A.R. Conceptualization was developed by A.R., M.G. and R.O. The methodology was developed by A.R., G.C., P.P. and R.O. Validation was performed by A.R., P.P. and G.C. Formal analysis was carried out by A.R. and S.J. Resources were provided by A.R. and R.O. The manuscript was written by A.R. and R.O., with review by all authors. Visualization was carried out by A.R. and G.C. Supervision was provided by A.R., M.G., S.J., A.K.K. and R.O.

Competing interests

The authors declare no competing interests.

Additional information

Methods

Sample fabrication. Commercial YAG (FOCtek Photonics; dimensions of $20 \times 10 \times 2$ mm^3 and crystal orientation <111>) and c-plane <0001> sapphire substrates were processed by means of standard 3DLW with an ytterbium mode-locked ultrafast fibre laser with 1,030 nm wavelength, 350 fs pulse duration, and linear polarization (Satsuma Amplitude Systèmes). The laser repetition rate for all experiments was set at 500 kHz, but trials at 1 MHz were found to yield qualitatively equal results (not shown here for the sake of brevity). A half-wave plate in combination with a linear polarizer was used to control the laser power, and a quarter-wave plate was used to convert linear polarization into circular polarization. A 1.4 numerical aperture (NA) oil-immersion Olympus objective was used to tightly focus the laser pulses inside the crystals. The working distance of the used objective was 0.15 mm, which limits to around 0.2 mm the maximum depth at which the material can be processed, given the refractive index of the crystal. Three-dimensional nanopositioning of the sample was performed by computer-controlled *XYZ* linear stages (ANT-series, Aerotech). Line scanning speeds were always 1 mm s^{-1} (but 2 mm s^{-1} in the case of the 1 MHz repetition rate).

After laser irradiation, the crystals were laterally polished to expose the irradiated structures and perform wet chemical etching. YAG crystals were etched in phosphoric acid (H_3PO_4 44 wt% solution) in deionized water. Etching was performed in a magnetic stirrer with a digital ceramic heating plate at 350 K (IKA C-MAG HS 4). Sapphire crystals were etched in 20 wt% hydrofluoric (HF) acid solution in deionized water at 308 K in an ultrasonic bath. After etching, the samples were cleaned in three consecutive ultrasonic baths with deionized water, acetone and methanol, respectively. In the case of YAG, no dependence on crystalline axis was found for the pore size and wet etching rate within our experimental resolution, so an arbitrary reference frame was set where x and y axes define the pore's cross-sectional plane, and z defines the pore length axis. The laser incoming direction was along the $-y$ axis in all figures. In the case of sapphire, laser fabrication experiments were performed with pores within the <0001> c plane in an arbitrary direction.

Wet etching of 3DLW nanostructures inside garnet crystals. Wet etching of garnets and other oxide crystals in hot phosphoric acid has been known since the 1960s[30]. The chemical reaction that may explain the wet dissolution of YAG has not been reported in the literature. A possible reaction could be

$$Y_3Al_5O_{12} + 8\ H_3PO_4 \rightarrow 3YPO_4 + 5AlPO_4 + 12H_2O$$
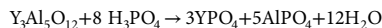
At this stage, we do not know what exact mechanism produces the observed etching selectivity at the molecular level within photo-modified and pristine YAG. However, due to the fact that very dense pore lattices can be fabricated with an absence of brittle fracture of samples (Fig. 3), we ascribe the ultrahigh etching selectivity between pristine and photo-modified regions to the creation of lattice defects at the laser ionized volumes in the absence of lattice phase changes to an amorphous YAG phase, which could entail crack propagation.

Garnets other than YAG are known to etch well in H_3PO_4 acid[30], and we expect that the present lithographic technique could also be valid for them. The use of yttrium iron garnet (YIG) crystals would be particularly interesting in photonic applications because of its higher index than YAG (2.20 for YIG and 1.81 for YAG, at 1,550 nm wavelength) as well as its well-known magneto-optical properties. Extension of the technique to other optical crystals such as sapphire was tested with similar ultrahighselectivity results (see next section).

Nanopore fabrication in sapphire crystals. Laser structuring of sapphire crystals has been a subject of research for more than a decade, with important seminal work done by Juodkazis and colleagues[21] that demonstrated the creation of microfluidic channels. Under the same 3DLW conditions as in YAG and circular laser polarization, nanopores with ~200 nm cross-section and millimetre-scale lengths were obtained in c-axis-cut sapphire substrates (Fig. 2). Nanopores were observed to form from a minimum laser power threshold of ~4 mW (significantly

lower than the observed threshold for YAG of ~7 mW; Supplementary Fig. 1a), for which an average width of 121 ± 12 nm and height of 135 ± 21 nm were measured, confirming that 3D nanolithography at the 100 nm level can also be achieved in sapphire (Fig. 2c).

In contrast with YAG, in sapphire we observed the appearance of multiple pores along the writing direction. We ascribe this in great part to birefringence-induced focus splitting in sapphire, in contrast to YAG, where this aberration is absent due to its index isotropy. Birefringence-induced focus splitting in 3DLW of crystals has been studied previously and occurs when focusing is performed at high NA along the optical c axis of the birefringent crystal[31]. We also disregard the possibility of a self-focusing mechanism being the origin of the observed focus splitting, due to the low pulse peak powers used in this technique (~0.05 MW) in comparison with the critical self-focusing power of ~3 MW for sapphire ($P_{cr} = 0.15\lambda^2/nn_2$, where $n \approx 1.74$ and $n_2 \approx 3 \times 10^{-16}$ cm^2 W^{-1}).

To etch laser-written sapphire crystals, both H_3PO_4 and HF acid solutions were tested, and only the latter produced observable etching of pores. The etching rate of nanopores was observed to be maximal for pores written at ~10 mW, for which an etching rate of 78.8 ± 0.7 μm h^{-1} was measured during the first hour of etching. The etching rate of unmodified sapphire was determined by measuring the difference in width and height of different pores etched for 40 h, and was determined to be <1 nm h^{-1} (0.34 ± 0.25 nm h^{-1}) on average.

Sample characterization. Back-scattered SEM was performed with a compact table-top SEM device on uncoated crystals at 10 kV (Phenom Pro, Phenom World). All images of air pore lattices were digitally processed with the open-source Fiji image processing package[32] to obtain all statistical size and shape distributions.

Fabricated subwavelength diffraction gratings were characterized at 1,070 nm with a fibre laser. A linear polarizer was used to set the polarization to transversal electric with respect to the grating, and a photodiode (PD300, OPHIR) was used to measure the power of the incoming, reflected, zero order and −1st diffracted order beams. MOWs were characterized at 1,310 nm and 1,550 nm with laser diodes and linear polarizers, and the imaging of the output modes of the MOWs was performed on an InGaAs camera with 640×512 pixels (Bobcat-640-GigE, Xenics). Free-space light in- and out-coupling from the MOWs was investigated with 0.68 and 0.55 NA aspheric lenses, respectively, which had an anti-reflection coating (1,050–1,600 nm) (C330TM-C, Thorlabs).

Theoretical calculations and simulation methods. The theoretical design of the subwavelength gratings was performed following the two-mode interference model developed by Clausnitzer and colleagues[27] for loss-less dielectric transmission gratings. The effective refractive indices of the grating were numerically simulated using the finite element method (FEM) in COMSOL Multiphysics 4.2. Perfectly matched layers were applied outside the computed regions to obtain open boundaries. The refractive index dispersion and Sellmeier coefficients of undoped YAG from the ultraviolet to mid-infrared ranges were taken from ref. [33]. Modelling of the YAG MOWs was also performed with the same FEM software and method.

Data availability

The data that support the plots within this paper and other findings of this study are available from the corresponding author upon reasonable request.

References

30. Basterfield, J. The chemical polishing of yttrium iron garnet. *J. Phys. D* **2**, 1159–1161 (1969).
31. Zhou, G. et al. Axial birefringence induced focus splitting in lithium niobate. *Opt. Express* **17**, 17970–17975 (2009).
32. Schindelin, J. et al. Fiji: an open-source platform for biological-image analysis. *Nat. Methods* **9**, 676–682 (2012).
33. Zelmon, D. E., Small, D. L. & Page, R. Refractive-index measurements of undoped yttrium aluminum garnet from 0.4 to 5.0 μm. *Appl. Opt.* **37**, 4933–4935 (1998).